Nanobubbles based on repeated compression for contrast-enhanced ultrasound (CEUS) imaging of renal fibrosis

Chenyi Zhang, Tiandong Chen, Fang Yang*

State Key Laboratory of Bioelectronics, Jiangsu Key Laboratory for Biomaterials and Devices, School of Biological Sciences and Medical Engineering, Southeast University, Sipailou 2, Nanjing, Jiangsu 210009, P. R. China

Abstract: Renal fibrosis, a crucial pathological process in chronic kidney disease, requires early precise diagnosis to delay renal failure. Traditional ultrasound has limitations in sensitivity and specificity. In this study, SF_6-loaded phospholipid nanobubbles (SF_6-NBs) were prepared by the repeated compression method and contain, which is used for renal fibrosis diagnosis. Results show that the optimized nanobubbles maintain good stability and biocompatibility. In renal fibrosis mouse models, after tail vein injection, the nanobubbles can effectively perfuse renal vessels at different levels, including interlobar arteries and cortical micro-arteries, thereby enhancing kidney ultrasound signals and clearly showing kidney structure and blood perfusion. Further experiments, including hemolysis tests, confirm the safety of nanobubbles, with no significant hemolysis or endothelial cell apoptosis. Our results show that this technology can enhance the visualization of renal micro-arteries, offering a reference for valid diagnosis of renal fibrosis.

1. Introduction

Chronic Kidney Disease (CKD) is a global health threat with rising prevalence, driven by its insidious progression and renal fibrosis as its central pathological hallmark[1]. Renal fibrosis, the terminal stage of various kidney injuries, involves collagen deposition and extracellular matrix (ECM) overproliferation, leading to irreversible structural and functional damage[2]. Early diagnosis and staging are critical to halt progression, yet current methods face limitations. Renal biopsy, the gold standard, is invasive and cannot provide real-time monitoring. Non-invasive alternatives like biomarkers lack sensitivity for fibrosis quantification, necessitating the development of high-resolution imaging technologies to address this unmet clinical need[3].

Ultrasonography is widely used for renal screening due to its non-invasiveness and real-time imaging capabilities. However, conventional ultrasound lacks resolution to visualize microscopic fibrosis features (e.g., collagen deposition). Microbubble contrast agents enhance tissue contrast *via* harmonic imaging but are limited by their size (1~10 μm), which restricts penetration into microvasculature and complex renal regions like the interstitium. These limitations highlight the urgent need for advanced contrast agents to enhance ultrasound's diagnostic potential. Nanobubbles (< 1 μm), with their unique advantages over microbubbles, offer a transformative solution[4]. Their nanoscale diameter (50~500 nm) enables seamless perfusion into microvasculature without causing blockage, accessing deeper tissues (e.g., renal interstitium) unreachable by traditional agents. This enables high-resolution imaging of fibrosis microstructures.

This study developed a novel SF_6-NBs contrast agent using a repeated compression methodology, which exhibited outstanding CEUS imaging capabilities in both *in vitro* and *in vivo* settings. The SF_6-NBs, characterized by their nanoscale dimensions and enhanced stability, showed effective perfusion of microvascular networks within the renal cortical region. In preclinical evaluations utilizing unilateral ureteral obstruction (UUO)-induced renal fibrosis mouse models, CEUS analysis revealed significant diagnostic efficacy, with fibrotic kidneys exhibiting markedly reduced peak signal intensities and slower descending slopes compared to healthy controls, reflecting impaired microvascular perfusion. The biosafety profile of the nanobubbles was collectively confirmed through comprehensive biocompatibility assessments, including calcein-AM/propidium iodide (PI) staining for cellular viability and hemolysis testing. These findings demonstrated that the SF_6-NBs can be used as a promising diagnostic platform for non-invasive assessment of renal fibrosis progression, offering a novel CEUS-based strategy to advance early-stage disease detection.

2. Materials and Methods

2.1. Materials

All solutions were prepared using filtered 18.2 MΩ deionized water (Direct-Q, Millipore, Billerica, MA). The gas used to prepare nanobubbles were sulfur hexafluoride

*yangfang2080@seu.edu.cn

(SF_6) with a purity of 99.99 wt%, which was purchased from Anhui Qiangyuan Gas Co., Ltd. (China). 1,2-distearoyl-sn-glycero-3-phosphocholine (DSPC) and 1,2-distearoyl-sn-glycero-3-phosphoethanolamine-N-[methoxy (polyethylene glycol)-2K] (DSPE-mPEG2K) were purchased from Dongnan Nano-Material (China).

2.2. Cell Culture

Human umbilical vein endothelial cells (HUVEC) were purchased from Wuhan Pricella Biotechnology (China). It was cultured in Dulbecco's Modified Eagle's Medium (DMEM) containing 10% fetal bovine serum (FBS) (Gibco, USA), 1% penicillin (Thermo Fisher Scientific, USA), and 1% streptomycin (Thermo Fisher Scientific, USA), and maintained in a 5% CO2 incubator at 37 °C with humidified atmosphere.

2.3. Preparation of SF_6-NBs

A mixture of phospholipids with a molar ratio of 9: 1 between DSPC and DSPE-mPEG2K were dissolved in 2 mL of hydration solution. Then, it was transferred to a 4 mL transparent vial and sealed with a rubber stopper and aluminum cap. A 5 mL syringe filled with 4 mL of SF_6 gas was inserted into the vial below the midpoint of the lipid solution. The vial was preheated in a 55°C water bath. Then, the syringe was reciprocally compressed 20 times to obtain SF_6-NBs.

2.4. Characterization of SF6-NBs

Morphological characterization of SF_6-NBs was performed using transmission electric microscopy (TEM, Talos F200X, 200 kV accelerating voltage, 0.25 nm point resolution, 0.12 nm information resolution, 0.16 nm STEM resolution) and scanning electric microscopy (SEM, 0.25 nm point resolution, 0.12 nm information resolution, 0.16 nm STEM resolution). SF_6-NBs were purified by low-speed centrifugation (1000 rpm, 10 min) to remove glycerol and propylene glycol. The supernatant was discarded, and the precipitate was resuspended in deionized water. This process was repeated for 3 times. For SEM analysis, 10 μL of diluted SF_6-NBs was dripped onto a silicon wafer and dried. Hydrodynamic size and bubble concentration were measured using a Beckman Coulter particle size analyzer with a 20 μm aperture tube. A 100 mL aliquot of physiological saline was added to the measurement beaker, followed by 50 μL of the bubble sample. Zeta potential was assessed using a dynamic laser light scattering and Zeta potential analyzer (Nano-ZS90). A 100 μL aliquot of the SF_6-NBs sample was diluted 40 times with pure water and analyzed.

2.5. CEUS imaging of SF_6-NBs *in vitro*

In accordance with established protocols outlined in the literature, the phantom preparation and subsequent *in vitro* ultrasonic imaging were conducted. The SF_6-NBs sample was subsequently introduced into this phantom. *In vitro* ultrasonic imaging was then performed using the probe of a small animal ultrasound imaging system (18 MHz, 20% power), allowing for the assessment of the sample's ultrasound enhancement capability within the tissue-mimicking phantom environment.

2.6. CEUS imaging of SF_6-NBs in kidney

A C57BL/6 mouse was prepared by first depilating the dorsal area using hair removal cream. Subsequent anesthesia was induced *via* a gas anesthesia machine, after which the mouse was secured onto the operating table. Ultrasound imaging of the renal region was performed using the probe of a small animal ultrasound system (VisualSonics Vevo 2100, Canada), following depilation of the target area. Adjust the instrument parameters to 18 MHz, 30% Power, and a frame rate of 10.

2.7. Data statistics

Quantitative data are expressed as the mean ± standard deviation (SD) of the sample number (n). Experimental data analysis was performed using OriginPro2018 software (USA). For statistical analysis, unpaired Student's t-tests were used for comparisons between two groups, while one-way ANOVA was employed for multiple comparisons. Statistical significance was determined by $^{*}P < 0.05$, indicating a significant difference; $^{**}P < 0.01$ and $^{***}P < 0.001$ indicate highly significant differences. If marked as ns, it indicates that the difference is not statistically significant. Quantitative analysis of fluorescence intensity in confocal images was performed using Image J software (USA) for density measurement.

3. Results and Discussion

3.1. Preparation and characterization of SF_6-NBs

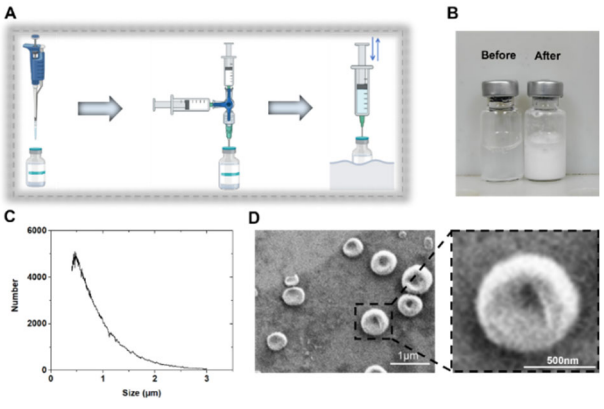

Figure 1. A) The basic steps of the repeated compression method include: encapsulation of lipid dispersion, gas pressurization and repeated compression. B) Photos of lipid dispersion and SF_6-NBs. C) The size distribution of SF_6-NBs. D) SEM images of SF_6-NBs.

Nanobubbles were prepared using repeated compression method base on our previous studies[5,6] (Figure 1A). The method produces a stable white dispersion, densely

packed with nanobubbles (Figure 1B). The mean size and concentration of the SF_6-NBs were measured with a size of appropriately 500 nm and a concentration of 1.32×10^{11} SF_6-NBs/mL (Figure 1C). Results of SEM revealed spherical, slightly concave shapes, confirming the nanobubble structure (Figure 1D).

3.2. *In vitro* CEUS imaging of SF_6-NBs

The *in vitro* CEUS capability of SF_6-NBs was evaluated using a small animal ultrasound imaging system. The SF_6-NBs were diluted 40-fold and positioned within a tissue-mimicking phantom to simulate *in vivo* acoustic conditions (Figure 2A). The CEUS imaging of SF_6-NBs revealed pronounced and sustained signal retention within the phantom over a 20-minute period, thereby confirming their enhanced contrast persistence and structural stability under in vitro conditions (Figure 2B). The signal intensity decreased from approximately 6000 to around 2500 after 20 minutes, retaining 41.7% of its original signal strength (Figure 2C). This result highlighted the potential of SF_6-NBs as a robust contrast agent with prolonged echogenicity in ultrasound applications.

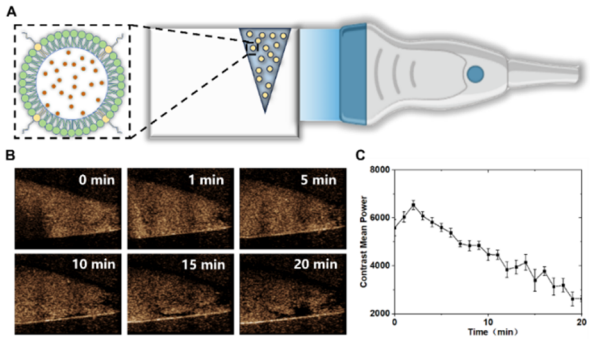

Figure 2. A) *In vitro* schematic illustration of CEUS imaging of SF_6-NBs using a tissue-mimicking phantom. B) *In vitro* ultrasound imaging of SF_6-NBs and C) the corresponding quantitative analysis.

3.3. *In vivo* CEUS imaging of SF_6-NBs

To validate the effective perfusion of SF_6-NBs in renal vasculature, *in vivo* CEUS of mouse kidneys was performed using an ultrasound imaging system (Figure 3A). The integration of Doppler imaging (Figure 3B) with CEUS (Figure 3C) was specifically employed to differentiate interlobar arteries from cortical micro-arteries within the renal vasculature for subsequent imaging analyses. As shown in Figure 3C, the signals first appeared in the large arteries of the renal cortex, then gradually extended into micro-arteries. Such temporal sequence is consistent with renal hemodynamic patterns, that is blood flow initially through large arteries before distributing to micro-arteries. The region of interest (ROI) analysis focusing on cortical micro-arteries regions showed the signal intensity rapidly increasing to approximately 2500 within 10 s followed by a subsequent decline to around 1000 by 20 s (Figure 3D). This temporal pattern showed the rapid perfusion and subsequent washout of SF_6-NBs within the intact cortical micro-arteries of healthy renal cortex. These findings demonstrated that SF_6-NBs can serve as an ideal ultrasound-responsive contrast agent for diagnostic applications in renal-related diseases such as renal fibrosis.

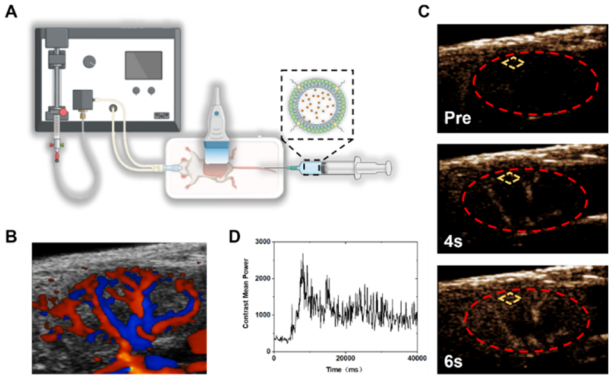

Figure 3. A) Schematic diagram illustrating the integrated operation of the small animal gas anesthesia system and the small animal ultrasound imaging system. B) Doppler ultrasound image of mouse kidney. C) CEUS imaging of kidney (red dashed lines) of healthy mouse. To detect renal microcirculatory perfusion, the micro-arteries (yellow dashed lines) were identified in the CEUS images and D) quantified through analysis of CEUS imaging signals.

3.4. CEUS imaging assessment of renal fibrosis progression in UUO mouse models

The UUO-induced renal fibrosis mouse model was employed to investigate the pathological alterations of renal microvasculature in renal fibrosis (Figure 4A). SF_6-NBs were administered *via* tail vein injection, and the renal cortical micro-arteries regions of mice were selected as ROI for CEUS imaging signal analysis at 24, 48, and 72 hours following UUO surgery (Figure 4B-D). As shown in Figure 4E, the relative peak signal intensity of SF_6-NBs in the renal cortex decreased to 1410.07 ± 136.81, 898.47 ± 267.34, and 669.54 ± 210.37 at 24, 48, and 72 h post-surgery, respectively (control group: 2442.98 ± 121.90). Concurrently, the contrast agent descending slope progressively declined to 0.0729 ± 0.0214, 0.0282 ± 0.0022, and 0.0181 ± 0.0032 at the same time points (control group: 0.1601 ± 0.0144) (Figure 4F). These dynamic changes indicated a progressive reduction in cortical perfusion volume coupled with prolonged SF_6-NBs retention time, which temporally aligned with the progression of renal fibrosis.

The observed perfusion decline is likely driven by early endothelial dysfunction and subsequent vascular remodeling. At 24 h post-UUO, inflammation and extracellular matrix (ECM) deposition impair endothelial nitric oxide bioavailability, increasing vascular resistance and limiting peak perfusion. Within 48~72 h, excessive collagen accumulation and vascular wall thickening further restrict vessel compliance, delaying SF_6-NBs washout. This CEUS-based assessment showed that the quantitative perfusion parameters and descending (washout) slope-correlate with dynamic vascular dysfunction, enabling longitudinal monitoring of fibrosis progression.

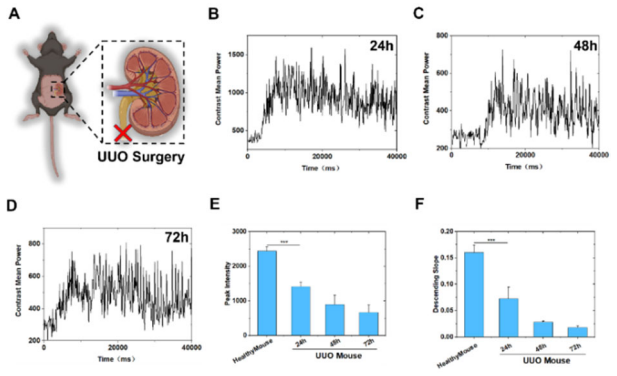

Figure 4. A) Schematic diagram illustrating the surgical procedure for establishing UUO-induced renal fibrosis in mice. Quantitative analysis of CEUS imaging of SF_6-NBs in the renal micro-arterial regions of mice at B) 24 h, C) 48 h, and D) 72 h post-UUO surgery. Quantitative analysis of E) peak intensities and F) descending slope of the signal in CEUS imaging of SF_6-NBs perfused renal micro-arteries at 24 h, 48 h, and 72 h post-UUO surgery.

3.5. Biosafety of SF_6-NBs

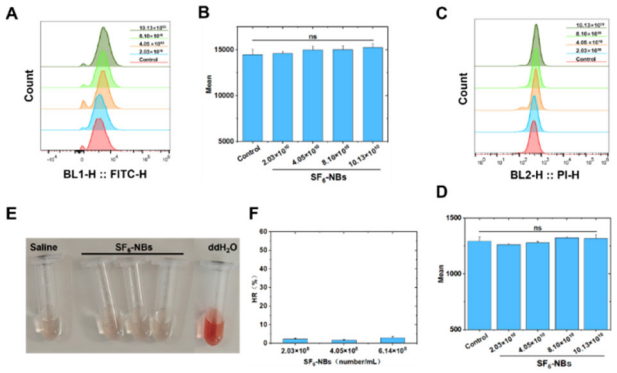

Figure 5. A) BL1-H: FITC-H flow histogram and B) the mean. C) BL2-H: PI-H flow histogram and D) the mean. E) Hemolysis test of SF_6-NBs and F) the quantitative analysis (n = 3).

After 12-h co-incubation with HUVECs at concentrations ranging from 2.03×10^{10} to 10.13×10^{10} SF_6-NBs/mL, no statistically significant differences were observed in live cell fluorescence (green, calcein-AM) (Figure 5A, B) or dead cell fluorescence (red, PI) (Figure 5C, D) between the control and experimental groups, demonstrating good cytocompatibility of SF_6-NBs. Furthermore, hemolysis assays demonstrated that SF_6-NBs exhibited blood compatibility comparable to physiological saline (negative control) across tested concentrations (2.03~6.14 $\times$ 10^{10} SF_6-NBs/mL). Supernatant color remained indistinguishable from the saline control without visible red discoloration (hemolysis marker) (Figure 5E). Quantitative analysis confirmed hemolysis rates of 1.78~3.04% (< 5%), statistically equivalent to the negative control (Figure 5F). These findings collectively validate the outstanding biocompatibility and hemocompatibility of SF_6-NBs within the tested concentration ranges.

4. Conclusion

This study successfully synthesized a novel SF_6-NBs contrast agent *via* a repeated compression method, demonstrating excellent CEUS imaging capabilities both *in vitro* and *in vivo*. The SF_6-NBs, characterized by their small size and superior stability, enabled effective perfusion of micro-arteries in the renal cortical region and achieved optimal CEUS imaging performance. In the analysis of UUO-induced renal fibrosis mouse models, CEUS imaging revealed significant reductions in both the peak intensity and the decay slope of the ultrasound signals in the renal cortical micro-arteries following UUO surgery. The biosafety of the SF_6-NBs was rigorously validated through calcein-AM/PI staining for cellular viability assessment and hemolysis assays, which confirmed their excellent biocompatibility. Collectively, this study presents a safe and effective nanobubble platform for CEUS diagnosis of renal fibrosis, providing a promising foundation for advancing non-invasive diagnostic strategies in renal fibrosis.

References

1. Li, L.; Fu, H.; Liu, Y. The Fibrogenic Niche in Kidney Fibrosis: Components and Mechanisms. *Nat. Rev. Nephrol.* **2022**, *18* (9), 545–557. https://doi.org/10.1038/s41581-022-00590-z.
2. Huang, R.; Fu, P.; Ma, L. Kidney Fibrosis: From Mechanisms to Therapeutic Medicines. *Signal Transduct. Target. Ther.* **2023**, *8* (1), 129. https://doi.org/10.1038/s41392-023-01379-7.
3. Klinkhammer, B. M.; Boor, P. Kidney Fibrosis: Emerging Diagnostic and Therapeutic Strategies. *Mol. Aspects Med.* **2023**, *93*, 101206. https://doi.org/10.1016/j.mam.2023.101206.
4. Li, J.; Xi, A.; Qiao, H.; Liu, Z. Ultrasound-Mediated Diagnostic Imaging and Advanced Treatment with Multifunctional Micro/Nanobubbles. *Cancer Lett.* **2020**, *475*, 92–98. https://doi.org/10.1016/j.canlet.2020.01.028.
5. Jin, J.; Yang, F.; Li, B.; Liu, D.; Wu, L.; Li, Y.; Gu, N. Temperature-Regulated Self-Assembly of Lipids at Free Bubbles Interface: A Green and Simple Method to Prepare Micro/Nano Bubbles. *Nano Res.* **2020**, *13* (4), 999–1007. https://doi.org/10.1007/s12274-020-2732-x.
6. Chen, T.; Miao, W.; Yang, Z.; Yang, F. From Nanovesicles to Nanobubbles Based on Repeated Compression Method. *Langmuir* **2023**, *39* (47), 16740–16749. https://doi.org/10.1021/acs.langmuir.3c01817.